 FDMP, vol.15, no.2, pp.89-105, 2019

Effect of Richardson Number on Unsteady Mixed Convection in a Square Cavity Partially Heated From Below

Sacia Kachi[1, *], Fatima-zohra Bensouici[1], Nawel Ferroudj[1] and Saadoun Boudebous[2]

Abstract: The objective of the present study is to analyze the laminar mixed convection in a square cavity with moving cooled vertical sidewalls. A constant flux heat source with relative length *l* is placed in the center of the lower wall while all the other horizontal sides of the cavity are considered adiabatic. The numerical method is based on a finite difference technique where the spatial partial derivatives appearing in the governing equations are discretized using a high order scheme, and time advance is dealt with by a fourth order Runge Kutta method. The Richardson number *(Ri)*, which represents the relative importance of the natural and forced convection, is chosen as the bifurcation parameter. The effect of this non-dimensional number on the behavior of the fluid flow and the heat transfer is analyzed. Although the geometry and boundary conditions concerning the velocity and the temperature are symmetrical with respect to the vertical axis passing through the center of the cavity, the results show the existence of symmetric and asymmetric flow structures, varying according to the considered value of the Richardson number.

Keywords: Richardson number, mixed convection, square cavity, finite difference method, bifurcation.

Nomenclature

g	gravitational acceleration, $m.s^{-2}$
Gr	Grashof number ($=g\beta q'' L^4/ k\nu^2$)
k	thermal conductivity, $W.m^{-1}. K^{-1}$
l	length of the heat source, m
L	length of the square cavity, m
n	normal direction
Nu(x)	dimensionless local Nusselt number
Nu_{av}	dimensionless average Nusselt number
Pr	Prandtl number, ($=\nu/\alpha$)
q''	Thermal flux density, $W.m^{-2}$

[1] Faculty of Process Engineering, University of Salah Boubnider Constantine 3, Algeria.

[2] Faculty of Sciences and Applied Sciences, University of Larbi BenM'hidi, Oum el Bouaghi, Algeria.

[*] Corresponding Author: Sacia Kachi. Email: kachi.sacia@gmail.com.

Re	Reynolds number, ($=V_0L/\nu$)
Ri	Richardson number ($=Gr/Re^2$)
t	time, s
T	absolute temperature, K
T_c	sidewall temperature, K
U	horizontal dimensionless velocity component
V_0	sidewall velocity, $m.s^{-1}$
V	vertical dimensionless velocity component
x, y	dimensional Cartesian coordinates, m
X, Y	dimensionless Cartesian coordinates (X =x/L, Y =y/L)

Greek symbols

α	thermal diffusivity, $m^2.\ s^{-1}$
β	thermal expansion coefficient, K^{-1}
ε	dimensionless length of the heat source
Θ	dimensionless temperature
ν	kinematic viscosity, $m^2.s^{-1}$
τ	dimensionless time
ψ	stream function, $m^2.s^{-1}$
Ψ	dimensionless stream function
ω	vorticity, s^{-1}
Ω	dimensionless vorticity

1 Introduction

Heat transfer by natural and mixed convection in confined spaces has attracted attention in recent years because of its importance, not only in the field of scientific academic research but also in industrial processes, as for example in cooling of electronic devices, heat exchangers, chemical reactors design, solar collectors, thermal storage system and many other applications. Numerous studies of natural and mixed convection within enclosures have been reported extensively in the literature that we can all mention here. Therefore, we focus on the convective flows in cavities partially or fully heated from below, with the particularity that the boundary conditions are strictly symmetric about the vertical axis through the center of the cavity. Most of these studies have revealed that dynamic and thermal behavior of the convective flows in such configurations are strongly dependent on both the enclosure geometry, the boundary conditions and the variation of several parameters including Reynolds, Prandtl and Rayleigh (or Grashof) numbers. It is well known that this high dependence can exhibit, in some cases, a large diversity of

complex dynamical and thermal behavior such as instability, symmetry breaking, bifurcation and chaos. A detailed review of the existing literature, in connection with the topic of this present study, can be subdivided into two categories, natural convection and forced/mixed convection.

In the first category the studies mentioned in the literature have concentrated, for the most part, on cavities heated partially or fully from below and cooled from above. The heated part is maintained either at a constant temperature or at a constant heat flux and all remaining boundaries are specified as adiabatic walls. Among these investigations, Robillard et al. [Robillard, Wang and Vasseur (1988); Hasnaoui, Bilgen and Vasseurt (1992)] demonstrated the existence of a large number of steady-state solutions depending on the aspect ratio, Rayleigh number, and dimensionless length of the heated segment. [Corcione (2003)] investigated the effects of the thermal boundary conditions at the sidewalls and noticed that the number of cells of the flow field increases as the width-to-height aspect ratio of the enclosure increases. D'Orazio et al. [D'Orazio, Cianfrini and Corcione (2004)] studied the effect of the aspect ratio of the cavity and the Rayleigh number on the behavior of the fluid flow. They show that as the Rayleigh number increases, the flow model evolves successively from a stable cell to two stable cells, then to one to three periodic cells and finally to three periodic cells. This evolution leads to abrupt or smooth changes in the Nusselt number. Venturi et al. [Venturi, Wan and Karniadakis (2010)] used different stochastic modeling approaches to study the bifurcation and stability process for specific values of the Rayleigh and Prandtl number. They conclude that this method captures accurately the onset of convective instability as well as multiple convection patterns corresponding to random initial flow states. Ngo et al. [Ngo and Byon (2015)] also consider the same cavity configuration as previously. Their work indicates that loss of symmetry can occur for all values of the heated part when the Rayleigh number is greater than 10^4. More recently, Bouabdallah et al. [Bouabdallah, Ghernaout, Teggar et al. (2016)] reported the numerical results of the natural Rayleigh-Benard convection in the rectangular cavities. Five bifurcation modes were detected, all dependent on the value of the Rayleigh number and the aspect ratio of the cavity. It should be noted that some authors have examined other geometric forms of cavities, such as isosceles triangular enclosures [Ridouane and Campo (2006); Varol, Oztop and Koca (2008)], prismatic enclosures [Aich, Hajri and Omri (2011); Saha and Gu (2015)], and trapezoidal enclosures [Tracy and Crunkleton (2012); Esfe, Arani, Yan et al. (2016)].

However, it is also possible to obtain, by studying natural convection in the similar geometric configurations, perfectly stable flows, without loss of symmetry and without bifurcations. Aydin et al. [Aydin and Yang (2000a), Saha, Saha, Islam et al. (2007); Sharif and Mohammad (2005)] studied numerically the natural convection in a square enclosure with centrally localized heating from below and symmetrical cooling from the sides. The bottom surface, except for the heated section, and the upper wall are considered adiabatic. The dimensionless length of the heat source investigated are 1/5, 2/5, 3/5 and 4/5 and the Rayleigh number is varied from 10^1 to 10^6. Calcagni et al. [Calcagni, Marsili and Paroncini (2005); Corvalo and Paroncini (2008)] investigated the same problem experimentally by using real-time and double-exposure holographic interferometry and numerically by using the commercial finite volumes code Fluent. More recently, Raisi [Raisi (2016)] examined the natural convection in a square cavity

filled with a non-Newtonian power-law fluid and used the numerical finite difference method based on the control volume formulation and SIMPLE algorithm. Certain studies have also been devoted to natural convection in other geometric configurations: Tzeng et al. [Tzeng, Liou and Jou (2005)] considered a triangular enclosure, Basak et al. [Basak, Roy, Singh et al. (2009)] treated a trapezoid enclosure, while Ahmanache et al. [Ahmanache and Zeraibi (2013); Alam, Rahman, Parvin et al. (2016)] examined a prismatic enclosure.

In this first category, relating to natural convection all studies cited above show that if the sidewalls of the cavity are adiabatic, instabilities, loss of symmetry and bifurcation phenomena have been found to depend mainly on Rayleigh numbers, aspect ratio and vertex angles of the enclosure. In contrast, when the sidewalls are isotherm the fluid flow does not exhibit any instability, loss of symmetry or bifurcations.

In the second category (mixed convection) when a difference in temperature is imposed the effect of the flow due to the buoyancy and displacement of the wall makes the analysis even more complex. The interaction of the sheared flow due to the movement of the wall and the flow of the natural convection due to the buoyancy effect is up to now a fundamental field of research and requires a complete analysis to understand the physics of the resulting flow and heat transfer. Aydin et al. [Aydin and Yang (2000b); Guo and Sharif (2004)] considered the numerical studies of the laminar mixed convection in a 2D cavity with an adiabatic upper wall and cold vertical walls moving downward at a constant velocity. A heat source is placed in the center of the lower wall. Guo et al. [Guo and Sharif (2004)] imposed a constant heat flux whereas [Aydin and Yang (2000b)] considered a fixed temperature wall and the remaining part of this wall is supposed to be adiabatic. The effects of the length of the heat source and the Richardson number were studied. In these two cases the effects of the forced and natural convection being co-operating, neither instabilities nor rupture of symmetry or bifurcation were observed.

The present study differs from Aydin et al. [Aydin and Yang (2000b); Guo and Sharif (2004)] in that here the direction of the displacement of the sidewalls are reversed thus creating a competition between the forced convection and the natural Rayleigh-Bénard convection. Therefore, it is interesting to establish the flow pattern and to predict the various critical values of the Richardson number for the occurrence of loss of symmetry and bifurcations, if these are indeed present in the fluid flow.

2 Model description

The physical model considered is depicted in Fig. 1. A square cavity whose sidewalls are maintained at fixed cold temperature T_c and move upwards with a fixed velocity V_0. A heat source maintained at constant heat flux q" and has a length l equal to 4/5 of L is placed in the center of the lower wall. All the other parts of the cavity are adiabatic. The flow in the cavity is induced by the force of shearing resulting from the movement of the side walls combined with the buoyancy force resulting from the heat source.

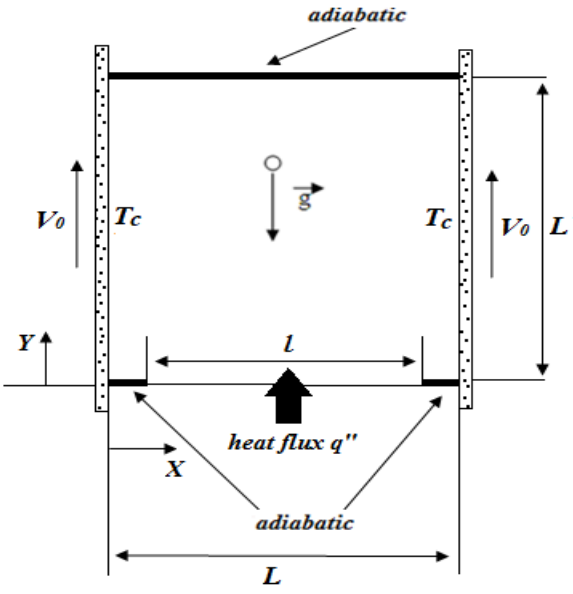

Figure 1: Schematic diagram of the physical model

3 Equations and mathematical expressions

The mixed convection phenomena to be investigated here are described by the complete Navier-Stokes and energy equations for two-dimensional laminar incompressible flow. The viscous dissipation term in the energy equation is neglected and the classical Boussinesq approximation is invoked for the buoyancy inducted body force term in the momentum equation. The 2-D governing equations are transformed into stream function-vorticity (Ψ-Ω) formulation and can be written in non-dimensional forms:

3.1 Energy transport equation

$$\frac{\partial \Theta}{\partial \tau} + U\frac{\partial \Theta}{\partial X} + V\frac{\partial \Theta}{\partial Y} = \frac{1}{RePr}\left[\frac{\partial^2 \Theta}{\partial X^2} + \frac{\partial^2 \Theta}{\partial Y^2}\right] \tag{1}$$

3.2 Vorticity transport equation

$$\frac{\partial \Omega}{\partial \tau} + U\frac{\partial \Omega}{\partial X} + V\frac{\partial \Omega}{\partial Y} = \frac{1}{Re}\left[\frac{\partial^2 \Omega}{\partial X^2} + \frac{\partial^2 \Omega}{\partial Y^2}\right] + Ri\frac{\partial \Theta}{\partial X} \tag{2}$$

3.3 Stream function equation

$$\frac{\partial^2 \Psi}{\partial X^2} + \frac{\partial^2 \Psi}{\partial Y^2} = -\Omega \tag{3}$$

3.4 Components of the velocity

$$U = \frac{\partial \Psi}{\partial Y} \quad V = -\frac{\partial \Psi}{\partial X} \tag{4}$$

The dimensionless vorticity is defined by:

$$\Omega = \frac{\partial V}{\partial X} - \frac{\partial U}{\partial Y}$$

where *Re*, *Pr* and *Ri* denote, respectively, Reynolds, Prandtl and Richardson numbers. They are defined as:

$$Re = \frac{V_0 L}{\nu} \qquad Pr = \frac{\nu}{\alpha} \qquad Ri = \frac{Gr}{Re^2}$$

The Grashof number *Gr* is expressed by:

$$Gr = \frac{g\beta q" L^4}{k\nu^2}$$

Here ν is the kinematic viscosity, α is the thermal diffusivity, β is the thermal expansion coefficient of the fluid and g represents the gravity acceleration and k is the thermal conductivity. The ratio Gr/Re^2 (Richardson number *Ri*) is a measure of the relative strength of the natural convection and forced convection and plays an important part to indicate the modes of convection. Dimensionless variables are given by the following expressions:

$$X = \frac{x}{L} \quad Y = \frac{y}{L} \quad U = \frac{u}{V_0} \quad V = \frac{v}{V_0} \quad \tau = t\frac{V_0}{L} \quad \Theta = \frac{k(T - T_c)}{q" L} \quad \Omega = \frac{L}{V_0}\omega \quad \Psi = \frac{\psi}{LV_0}$$

The numerical resolution of the previous equations is based on the following initial and boundary conditions:

- The initial conditions (τ=0) are:

$$0 < Y < 1 \;\; \& \;\; 0 < X < 1: \qquad \Theta = 0 \quad \Psi = 0 \quad \Omega = 0$$

- The boundary conditions (τ>0) are:

$$\left.\begin{matrix} X = 0 \\ X = 1 \end{matrix}\right\} \;\& \;\; 0 \le Y \le 1 \quad \Rightarrow U = \Theta = \Psi = 0 \quad V = 1. \tag{5a}$$

$$Y = 0 \quad \& \quad 0 \le X \le (1-\varepsilon)/2 \;\&\; (1+\varepsilon)/2 \le X \le 1 \qquad \Rightarrow U = V = \Psi = 0 \quad \frac{\partial \Theta}{\partial Y} = 0 \tag{5b}$$

$$Y = 0 \quad \& \quad (1-\varepsilon)/2 \le X \le (1+\varepsilon)/2 \qquad \Rightarrow U = V = \Psi = 0 \quad \frac{\partial \Theta}{\partial Y} = -1. \tag{5c}$$

$$Y = 1 \quad \& \quad 0 \le X \le 1 \quad \Rightarrow U = V = \Psi = 0 \quad \frac{\partial \Theta}{\partial Y} = 0 \tag{5d}$$

where $\varepsilon = l/L$ is the dimensionless length of the heat source.

Wall vorticity is evaluated by the development of first order Taylor series, which is a function of the stream function and the walls velocity. The expressions are:

$$\Omega_{i,w}^{bottom} = \frac{2}{\Delta Y_0^2}\left(\Psi_{i,w} - \Psi_{i,w+1}\right)$$

$$\Omega_{i,w}^{top} = \frac{2}{\Delta Y_0^2}\left(\Psi_{i,w} - \Psi_{i,w-1}\right)$$

$$\Omega_{w,j}^{left} = \frac{2}{\Delta X_0^2}\left(\Psi_{w,j} - \Psi_{w+1,j} - \Delta X_0\right)$$

$$\Omega_{w,j}^{right} = \frac{2}{\Delta X_0^2}\left(\Psi_{w,j} - \Psi_{w-1,j} + \Delta X_0\right)$$

where index w denotes the node located just on the wall, *i* and *j* are node locations in the *X* and *Y* directions, respectively. The first grid spacing in the *X* and *Y* directions are denoted by ΔX_0 and ΔY_0, respectively.

4 Numerical method

4.1 Discretization

The system of Eqs. (1)-(4), together with the boundary conditions Eqs. 5(a)-5(d) have been discretized and solved using the finite difference method. For solving nonlinear systems of differential partial equations, the fourth-order Runge-Kutta method is known to be quite effective compared to other methods. The convective terms in Eqs. (1)-(2) are discretized using the accurate third order upwind scheme of Kawamura et al. [Kawamura, Takami and Kuwahara (1985)] taking into account the sign of the velocity. A fourth-order centered scheme was adopted for the discretization of the diffusive terms, the source term in Eq. (2), and the explicit evaluation of the *U* and *V* components of the velocity vector in Eq. (4). The mirror-point technique due to Leonard [Leonard (1979)] was used to maintain the fourth-order centered scheme of the first and second spatial partial derivatives in the grid points adjacent to the walls. An iterative procedure based on successive Non Linear Over Relaxation method (NLOR) was used to solve the discretized stream function Eq. (3) in each time step of Runge-Kutta procedure. The iterative procedure is stopped when the maximum relative change in stream function between two consecutive iterations is less than 10^{-6}.

The dimensionless local and average Nusselt numbers of the hot part of the bottom wall are defined, respectively by Guo et al. [Guo and Sharif (2004)]:

$$Nu(X) = \frac{1}{\Theta_w(X)} \;;\; Nu_{av} = \frac{1}{\varepsilon}\int_0^{\varepsilon} Nu(X)\,dX$$

The average Nusselt number (Nu_{av}) is integrated using Simpson's rule.

4.2 Grid independence test

Grid independence tests were carried out. Computed results of dimensionless average Nusselt number, maximal stream function and temperature with *Ri*=10, *Re*=100 and *Pr*=0.71 obtained using different grid sizes are given in Tab. 1. It is observed that the values of these different variables do not show significant differences between them. The maximum relative error of these different variables for the grid sizes of 81×81, 101×101

and 161×161 compared to the grid size of 201×201 is about 2%, except that of the stream function which is in the order of 7%. In addition to that, the evolution of the average Nusselt number, for the same grid sizes, is shown in Fig. 2. On can see that the curve corresponding to the 101×101 mesh is close to those corresponding to 161×161 and 201×201. As a compromise between accuracy and CPU time, it was decided to use a non-uniform grid with 101×101 grid points for subsequent calculations.

Table 1: Effect of the grid arrangements on numerical solution

Grid sizes	81×81	101×101	161×161	201×201
Nu_{av}	5.65734	5.66724	5.68334	5.68913
ψ_{max}	7.8832×10^{-2}	8.1470×10^{-2}	8.5896×10^{-2}	8.7527×10^{-2}
Θ_{max}	0.1758	0.1772	0.1790	0.1797

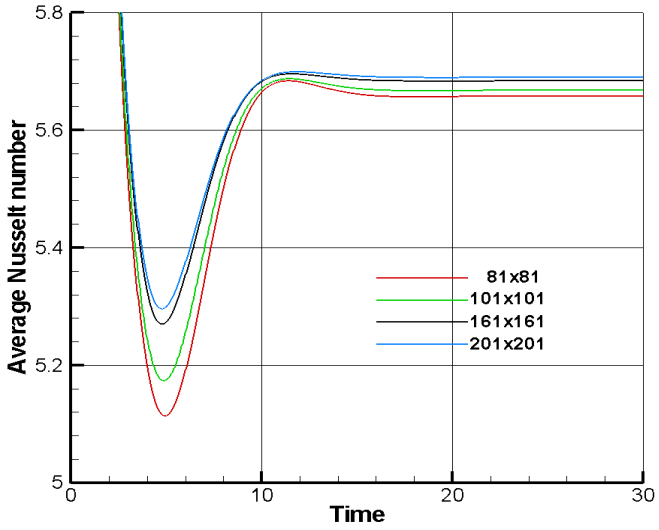

Figure 2: Evolution of the average Nusselt number for the different grid sizes

4.3 Code validation

The computer code developed with Fortran language has been validated by considering the geometric configuration investigated by Aydin et al. [Aydin and Yang (2000)]. We report in Fig. 3 and Fig. 4, a comparison of the average Nusselt number Nu_{av} of the heat source and the dimensionless vertical velocity profiles, at the horizontal mid-plane respectively. As can be noticed from these figures the obtained results show a good agreement between both models.

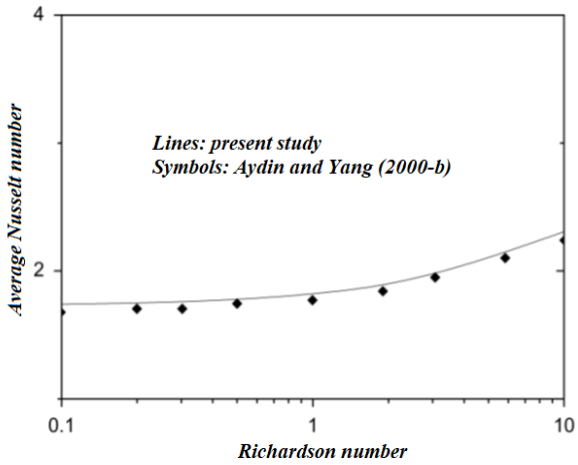

Figure 3: Comparison of the average Nusselt number Nu_{av} with results of Aydin et al. [Aydin and Yang (2000b)]

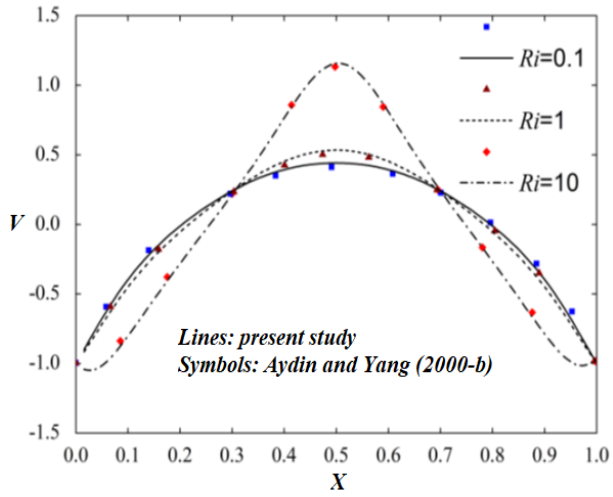

Figure 4: Comparison of the vertical component velocity V at Y=0.5 with results of Aydin et al. [Aydin and Yang (2000b)]

5 Results and discussion

In this study, the fluid flow and heat transfer phenomena are investigated for a wide range of Richardson numbers to detect various behaviors of the fluid flow in the cavity. Air was the working fluid with a constant Prandtl number of 0.71. The Reynolds number was fixed at 10^2 and the value of the Grashof number is between 5×10^3 and 10^6 depending on the value of the Richardson number.

5.1 Effect of Richardson number

The results of the effect of increasing the Richardson number on the average Nusselt number for the different simulations are shown in Fig. 4. It can be observed that the average Nusselt number along the bottom heated wall of the cavity increases continuously with increasing *Ri*. However, three different behaviors of the fluid flow may be observed from this figure. To show these two bifurcations, stream functions (above the curve) and isotherms contours (below the curve) are plotted on the same figure for Richardson numbers equal to 10, 35 and 45. A first bifurcation is located at point B while a second is located at point C. Point B marks the transition from a flow characterized by two perfectly symmetrical cells to a flow characterized by two asymmetrical cells, and point C indicates the passage of the previous flow to a flow characterized by two pairs of perfectly identical cells.

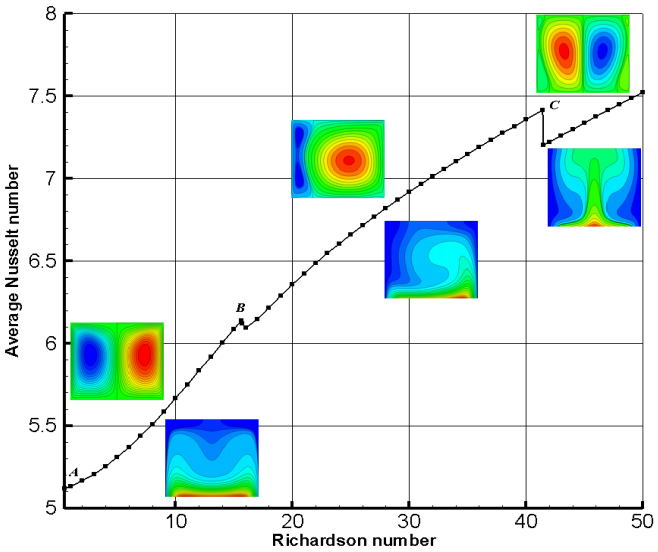

Figure 5: Variation of the average Nusselt number Nu_{av} with Richardson number *Ri*

5.2 First bifurcation

The first bifurcation occurs at point B (Fig. 5), when the Richardson number *Ri* increases from 15.6 to 15.7 and the Nu_{av} decreases abruptly from 6.14 to 6.12. Visual examination of the streamlines indicated in Fig. 6 shows a slight difference of the flow behavior before and after the first bifurcation. However, a slightly more pronounced asymmetry was observed in the isotherms shown in Fig. 7. In each case, we note that thermal stratification exists near the heated part. The ascending movement of the sidewalls leads upwardly adjacent fluid layers to the walls by viscous forces; we also note that the cold temperature prevails in the whole upper part of the cavity. In fact, the low heat flow recovered by the fluid from the heat source is directly discharged through the lower portion of the vertical walls.

Therefore, the temperature distribution is not affected by the increase of *Ri*; this justifies the dominance of shear forces with respect to buoyancy forces. Moreover, it is also visible in Fig. 6(b) and Fig. 10(a) that the right cell becomes progressively larger than the left, probably because the thermal boundary condition effect begins to generate a loss of symmetry of the fluid flow in the cavity. It is interesting to note that this asymmetry of the flow regime becomes more noticeable with the increase in *Ri* until it reaches the limit value of 41.4.

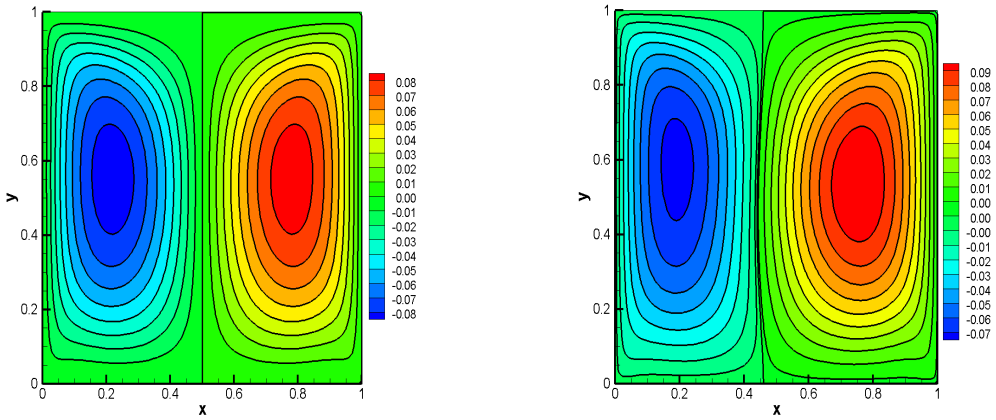

(a) (b)

Figure 6: Streamlines for *Ri*=15.6 (a) and *Ri*=15.7 (b)

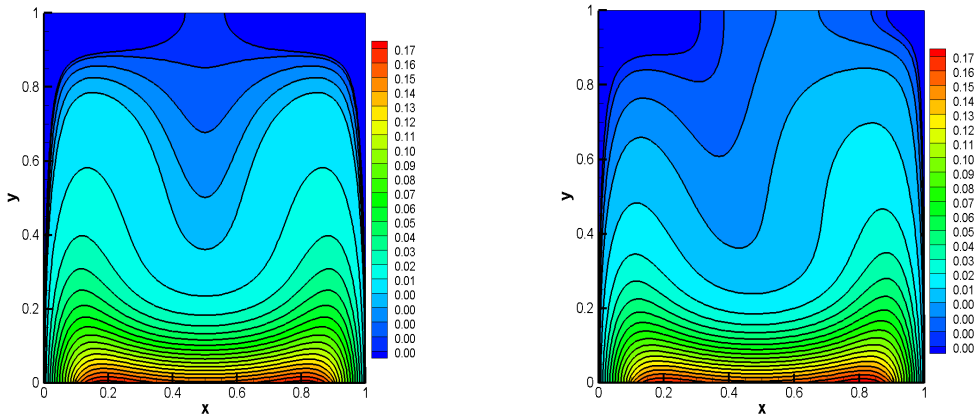

(a) (b)

Figure 7: Isotherms for *Ri*=15.6 (a) and *Ri*=15.7 (b)

The change in the flow behavior in this first bifurcation is depicted more clearly in Fig. 8, which shows the evolution of the Nu_{av} along the hot surface (Fig. 8(a)) and the temperature at the center of the cavity (Fig. 8(b)). We can see that the value of the Nu_{av} remains constant and equal to 6.14 at *Ri*=15.6, while for *Ri*=15.7 the value of the same number begins to decrease gradually at $\tau=12.5\times10^3$ and becomes stable and equal to 6.12

at τ=22.5×10^3. At the same time, the temperature computed at the center of the cavity increases gradually from 3.2×10^{-3} to 4.2×10^{-3}. It is obvious that if the standard test of convergence is applied to stop the calculations, the solution would have converged at τ=15, but the results obtained in the Fig. 7, for *Ri*=15.7, indicates that the change in fluid flow begins to occur at τ=12.5×10^3 to be stabilized at τ=22.5×10^3. It took a calculation time of between 2 and 3 days for each numerical simulation, while the Richardson number *Ri* is between 15 and 16, on a "HP Z820 Workstation" to detect this first bifurcation. In this case the corresponding number of iterations can reach about 225 million with a time step $\Delta\tau$ equal to 10^{-4}.

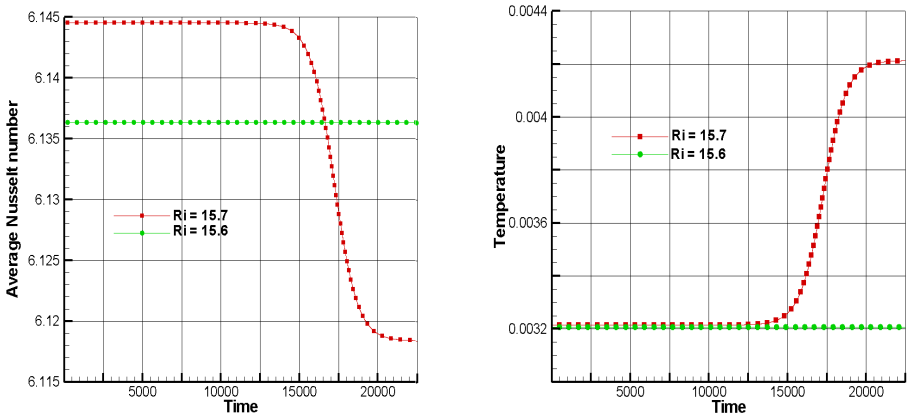

(a) (b)

Figure 8: Evolution of the Nu_{av} (a) and the temperature at the center of the cavity (b) for *Ri*=15.6 and 15.7

5.3 Second bifurcation

The second bifurcation occurs at point C (Fig. 5), when the Richardson number *Ri* increases from 41.4 to 41.5 the number of Nusselt decreases suddenly from 7.42 to 7.20. Fig. 9 and Fig. 10 show the dynamic and thermal fields for Richardson numbers equal to 41.4 and 41.5 respectively. It is interesting to observe that before and after this second bifurcation, the behavior of the flow in the cavity becomes radically different. Indeed, it goes from a state characterized by two unbalanced cells to a state characterized by two pairs of cells perfectly symmetrical. The pair of contra rotating cells in the center of the cavity is mainly managed by the buoyancy forces and viscous forces maintain the pair of clamped cells close to vertical moving walls (Fig. 9(b)). In this flow regime, the heat recovered from the heat source is conveyed by convection, in the form of a thermal plume, to the top of the cavity by the pair of cells in the center. This is what explains the relatively high temperatures in the central portion of the cavity. The heat is dissipated fairly through the two sidewalls (Fig. 10(b)).

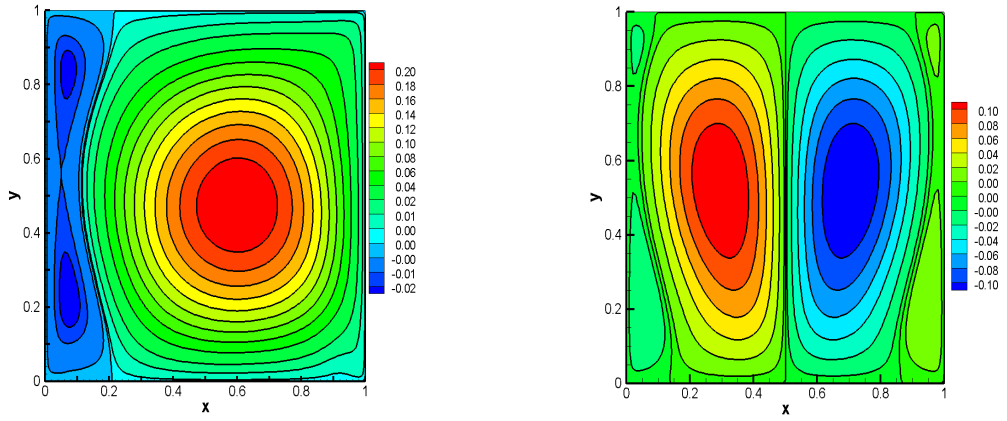

(a) (b)

Figure 9: Streamlines for *Ri*=41.4 (a) and *Ri*=41.5 (b)

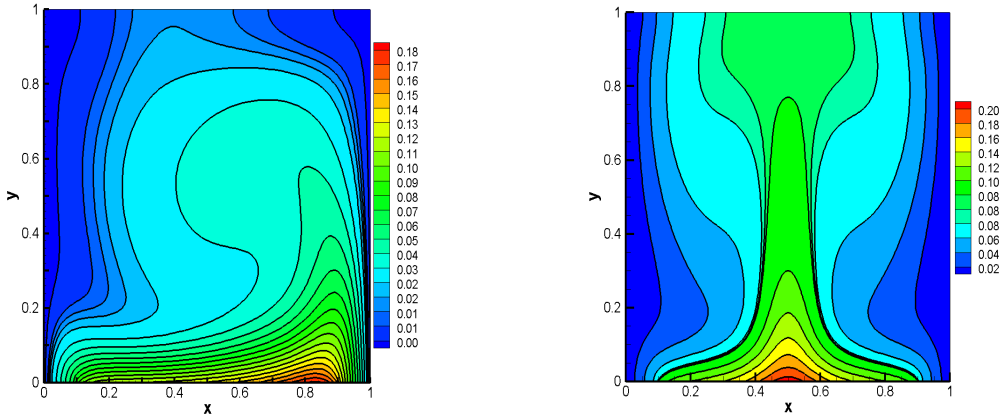

(a) (b)

Figure 10: Isotherms for *Ri*=41.4 (a) and *Ri*=41.5 (b)

The evolution of the average Nusselt number and the component *U* of the velocity at the center of the cavity are shown in Fig. 11 and Fig. 12 respectively. The value of the average Nusselt number (Fig. 11) fluctuates during the first instants (τ<20) and then decreases progressively to be stabilized at a fixed value equal to 7.20 for *Ri*=41.5, while for *Ri*=41.4, it presents an oscillation between τ=30 and τ=70 before being stabilized at a fixed value equal to 7.41. Unlike the first bifurcation, we found it useful to highlight the asymmetry of the fluid flow, not considering the temperature computed at the center of the cavity, but by plotting in Fig. 12 the quantitative evolution of the horizontal component *U* of the velocity computed at the same point (*X*=0.5, *Y*=0.5). A closer examination of this figure reveals that for *Ri*=41.5 the *U* component remains constant equal to 0 indicating no fluid passing through the vertical center plane, while for *Ri*=41.4 it fluctuates, then increases, afterwards gradually decreases to be stabilized at a negative

value equal to -0.7. As expected from Fig. 9(a) more fluid is transferred from the right side of the cavity to its left side.

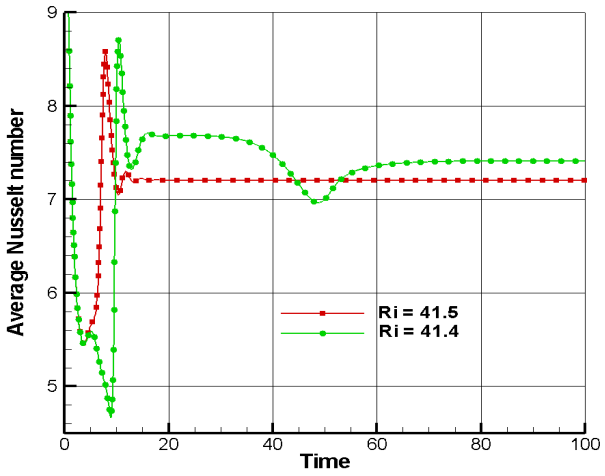

Figure 11: Evolution of the average Nusselt number for *Ri*=41.4 and 41.5

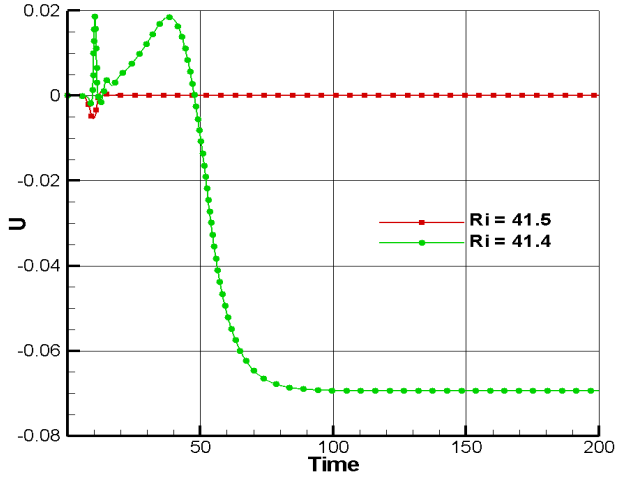

Figure 12: Evolution of the component U of the velocity at the center of the cavity for *Ri*=41.4 and 41.5

6 Conclusion

This study investigates numerical unsteady laminar mixed convection in a square cavity with constant heat flux applied on a part of the bottom wall. The sidewalls of the cavity are subjected to a constant cold temperature and a fixed upward velocity. The other parts of the cavity are considered adiabatic. The finite difference method was used to discretize the equations governing the studied phenomenon. The numerical results are obtained for different values of the Richardson number. Reynolds and Prandtl numbers are kept constant at values equal to 100 and 0.71 respectively.

In the confined flow, a competition between the shearing forces resulting from the movement of the sidewalls combined with the buoyancy forces resulting from the heat source may be at the origin of the bifurcation phenomena. The results of different numerical simulations carried out clearly indicate the existence of two bifurcations occurring in the given geometry. The first bifurcation is located at a Richardson number between 15.6 and 15.7 and the second bifurcation is between the values 41.4 and 41.5 of the same number. In the first bifurcation, the resulting flow consists of the transition from two symmetric counter-rotating vortices to two asymmetric counter-rotating vortices. In the second bifurcation, the resulting flow consists of the transition from two asymmetric counter-rotating vortices to four symmetrical counter-rotating vortices.

A particular feature in this study is related to the total absence of an a priori knowledge of the existence of bifurcations since the boundary conditions adopted here are perfectly symmetrical. These bifurcations would not have been revealed, if we had considered half the domain, with the symmetry condition on the vertical axis passing through the center of the cavity and if we had used the classic test of convergence of the solution to stop the calculations. This would have led to erroneous conclusions about the behavior of the fluid flow and the inability to find the non-symmetric solutions.

Acknowledgement: The authors like to express their thankfulness to the Laboratory of micro-systems and instrumentation, University of Mentouri brothers Constantine, for providing computer facility during this work.

References

Ahmanache, A.; Zeraibi, N. (2013): Numerical study of natural melt convection in cylindrical cavity with hot walls and bottom sink. *Thermal Science*, vol. 17, pp. 853-864.

Aich, W.; Hajri, I.; Omri, A. (2011): Numerical analysis of natural convection in a prismatic enclosure, *Thermal Science*, vol. 15, pp. 437-446.

Alam, M. S.; Rahman M. M.; Parvin, S.; Vajravelu K. (2016): Finite element simulation for heat line visualization of natural convective flow and heat transfer inside a prismatic enclosure. *International Journal of Heat and Technology*, vol. 34, pp. 391-400.

Aydin, O.; Yang, W. J. (2000a): Natural convection in enclosures with localized heating from below and symmetrical cooling from sides. *International Journal of Numerical Methods for Heat & Fluid Flow*, vol. 10, pp. 518-529.

Aydin, O.; Yang, W. J. (2000b): Mixed convection in cavities with a locally heated lower wall and moving sidewalls. *Numerical Heat Transfer, Part A: Applications*, vol. 36, pp. 695-710.

Basak, T.; Roy, S.; Singh, A.; Balakrishnan A. R. (2009): Natural convection flows in porous trapezoidal enclosures with various inclination angles. *International Journal of Heat and Mass Transfer*, vol. 52, pp. 4612-4623.

Bouabdallah, S.; Ghernaout, B.; Teggar, M.; Benchatti, A.; Benarab, F. Z. (2016): Onset of natural convection and transition laminar-oscillatory convection flow in Rayleigh-Bénard configuration. *International Journal of Heat and Technology*, vol. 34, pp. 151-157.

Calcagni, B.; Marsili, F.; Paroncini, M. (2005): Natural convective heat transfer in square enclosures heated from below. *Applied Thermal Engineering*, vol. 25, pp. 2522-2531.

Corcione, M. (2003): Effects of the thermal boundary conditions at the sidewalls upon natural convection in rectangular enclosures heated from below and cooled from above. *International Journal of Thermal Sciences*, vol. 42, pp. 199-208.

Corvalo, F.; Paroncini, M. (2007): Experimental analysis of natural convection in square cavities heated from below with 2D-PIV and holographic interferometers techniques. *Experimental Thermal and Fluid Science*, vol. 31, pp. 721-739.

Corvalo, F.; Paroncini, M. (2008): A numerical and experimental analysis on the natural convective heat transfer of a small heating strip located on the floor of a square cavity. *Applied Thermal Engineering*, vol. 28, pp. 25-35.

D'Orazio, M. C.; Cianfrini, C.; Corcione, M. (2004): Rayleigh-Bénard convection in tall rectangular enclosures. *International Journal of Thermal Sciences*, vol. 43, pp. 135-144.

Esfe, M. H.; Arani, A. A. A.; Yan, W. M.; Ehteram, H.; Aghaie, A. et al. (2016): Natural convection in a trapezoidal enclosure filled with carbon nano tube-EG-water Nano fluid. *International Journal of Heat and Mass Transfer*, vol. 92, pp. 76-82.

Guo, G.; Sharif, M. A. R. (2004): Mixed convection in rectangular cavities at various aspect ratios with moving isothermal sidewalls and constant flux heat source on the bottom wall. *International Journal of Thermal Sciences*, vol. 43, pp. 465-475.

Hasnaoui, M.; Bilgen, E.; Vasseurt, P. (1992): Natural convection heat transfer in rectangular cavities partially heated from below. *Journal of Thermo Physics and Heat Transfer*, vol. 6, pp. 255-264.

Kawamura, T.; Takami, H.; Kuwahara, K. (1985): New higher-order upwind scheme for incompressible Navier-Stokes equations. *Numerical Methods in Fluid Dynamics, Lecture Notes in Physics*, vol. 218, pp. 291-295.

Leonard, B. P. (1979): A stable and accurate convective modeling procedure based on quadratic upstream interpolation. *Computational Methods Applied Mechanical Engineering*, vol. 19, pp. 58-98.

Ngo, I. L.; Byon, C. (2015): Effects of heater location and heater size on the natural convection heat transfer in a square cavity using finite element method. *Journal of Mechanical Science and Technology*, vol. 29, pp. 2995-3003.

Raisi, A. (2016): Natural convection of non-newtonian fluids in a square cavity with a localized heat source. *Journal of Mechanical Engineering*, vol. 4, pp. 553-564.

Ridouane, E. H.; Campo, A. (2006): Formation of a pitchfork bifurcation in thermal convection flow inside an isosceles triangular cavity. *Physics of Fluids*, vol. 18, no. 7.

Robillard, L.; Wang, C. H.; Vasseur, P. (1988): Multiple steady states in a confined porous medium with localized heating from below. *Numerical Heat Transfer*, vol. 13, pp. 91-110.

Saha, G.; Saha, S.; Islam, M. Q.; Akhanda, M. A. R. (2007): Natural convection in enclosure with discrete isothermal heating from below. *Journal of Naval Architecture and Marine Engineering*, vol. 4, pp. 1-13.

Saha, S. C.; Gu, Y. T. (2015): Natural convection in a triangular enclosure heated from below and non-uniformly cooled from top. *International Journal of Heat and Mass Transfer*, vol. 80, pp. 529-538.

Sharif, M. A. R.; Mohammad, T. R. (2005): Natural convection in cavities with constant flux heating at the bottom wall and isothermal cooling from the sidewalls. *International Journal of Thermal Sciences*, vol. 44, no. 9, pp. 865-878.

Tracy, N. I.; Crunkleton, D. W. (2012): Oscillatory natural convection in trapezoidal enclosures. *International Journal of Heat and Mass Transfer*, vol. 55, pp. 4498-4510.

Tzeng, S. C.; Liou J. H.; Jou, R. Y. (2005): Numerical simulation-aided parametric analysis of natural convection in a roof of triangular enclosures. *Heat Transfer Engineering*, vol. 26, pp. 69-79.

Varol, Y.; Oztop, H. F.; Koca, A. (2008): Entropy production due to free convection in partially heated isosceles triangular enclosures. *Applied Thermal Engineering*, vol. 28, pp. 1502-1513.

Venturi, D.; Wan, X.; Karniadakis, G. E. (2010): Stochastic bifurcation analysis of Rayleigh-Bénard convection. *Journal of Fluid Mechanical*, vol. 650, pp. 391-413.